

Toward resolving small-scale structures in ionospheric convection from SuperDARN

R. André, J.-P. Villain, Catherine Senior, Laurent Barthès, C. Hanuise, Jean-Claude Cerisier, A. Thorolfsson

▶ **To cite this version:**

R. André, J.-P. Villain, Catherine Senior, Laurent Barthès, C. Hanuise, et al.. Toward resolving small-scale structures in ionospheric convection from SuperDARN. Radio Science, 1999, 34 (5), pp.1165-1176. 10.1029/1999RS900044 . insu-02186326

HAL Id: insu-02186326
https://insu.hal.science/insu-02186326

Submitted on 17 Jul 2019

HAL is a multi-disciplinary open access archive for the deposit and dissemination of scientific research documents, whether they are published or not. The documents may come from teaching and research institutions in France or abroad, or from public or private research centers.

L'archive ouverte pluridisciplinaire **HAL**, est destinée au dépôt et à la diffusion de documents scientifiques de niveau recherche, publiés ou non, émanant des établissements d'enseignement et de recherche français ou étrangers, des laboratoires publics ou privés.

Radio Science, Volume 34, Number 5, Pages 1165–1176, September–October 1999

Toward resolving small-scale structures in ionospheric convection from SuperDARN

R. André, [1] J.-P. Villain, [1] C. Senior, [2] L. Barthes, [2] C. Hanuise,[3] J.-C. Cerisier,[2] and A. Thorolfsson [2]

Abstract. The combination of radial velocities measured by a pair of Super Dual Auroral Radar Network (SuperDARN) HF coherent radars gives, in their common field of view, the velocity vectors in a plane perpendicular to the magnetic field. The standard merging is based on a natural grid defined by the beam intersections, which provides a resolution varying between 90 and 180 km (depending upon the distance to the radars). This allows the description of structures with a typical scale size (L) of the order of 500 km. The present study is devoted to a merging method which takes advantage of individual radar grids to enhance the resolution ($L \approx 200$ km). After a brief description of the standard merging method, we define the high-resolution grid and discuss the potential problems which have to be overcome. The first problem concerns the localization of the scattering volume, whereas the second one deals with the independence of the velocity vectors. These two limitations have been addressed in previous studies [*André et al.*, 1997; *Barthes et al.*, 1998]. In the method proposed here, several velocity vectors are determined at each grid point, from which the selection is made by using the hypothesis of minimization of the divergence magnitude. The selected map is the one which minimizes the divergence. The performances are tested and compared to the standard merging algorithm through simulated double vortices. Finally, we apply this method to real data, and show, through two examples, its ability to describe small-scale structures ($L \approx 200$ km).

1. Introduction

The combination of radial velocities measured by a pair of HF coherent radars gives, in their common field of view, the velocity vectors in a plane perpendicular to the magnetic field. Super Dual Auroral Radar Network (SuperDARN) radars [*Greenwald et al.*, 1995a] are able to determine the radial velocities in 16 different directions and 70 range gates. In the basic mode of operation the radial resolution is 45 km. Currently, velocity vectors are computed at the natural grid points defined by the beam intersections. The associated velocity map thus contains 256 potential vectors. This technique leads to a spatial resolution varying between 90 and 180 km depending upon distance to the radar.

These maps have been used for studies of large-scale structures (characteristic scale length approximatively equal to 500 km) in the ionospheric convection, such as vortices [*Bristow et al.*, 1995; *Greenwald et al.*, 1995b, 1996], but they cannot describe smaller-scale structures ($L \approx 200$ km). There is a need to resolve these small-scale structures, which are thought to be associated with reconnection at the cusp [*Rodger and Pinnock*, 1997] or on the nightside, in relation with substorm activity [*Yeoman and Luhr*, 1997; *Lewis et al.*, 1997].

The purpose of this paper is to present an algorithm which provides a high spatial resolution map of

[1]Laboratoire de Physique et Chimie de l'Environnement, CNRS, Orléans, France.

[2]Centre d'Etude des Environnements Terrestres et Planétaires, CNRS, Saint-Maur, France.

[3]Laboratoire de Sondage Electromagnétique de l'Environnement Terrestre, CNRS, Université de Toulon, La Garde, France.

Copyright 1999 by the American Geophysical Union.

Paper number 1999RS900044.
0048-6604/99/1999RS900044$11.00

the ionospheric convection. This spatially improved resolution is based on a grid determined by the radial resolution of the measurements, i.e., 45 km in the standard radar operating mode. In section 2, we briefly review the standard method presently used to compute velocity vector maps with one pair of radars. We discuss the advantages and limitations of this grid and the intrinsic difficulties related to a high-resolution grid. We then discuss the approach used to overcome these problems and present the global analysis conducted to compute this high-resolution map. Using simulated data, we illustrate the performances of this technique and demonstrate its ability to describe structures with a typical scale length of the order of 200 km. In section 3, this method is applied to real SuperDARN data containing a convection reversal and a vortex. We demonstrate that the vector maps preserve the resolution of the radial velocity maps of each radar.

2. Toward a High-Resolution Map

Before presenting the high-resolution merging algorithm, we briefly review the method used routinely for SuperDARN data, which was described by *Cerisier and Senior* [1994]. We then discuss the problems arising from the choice of the high-resolution grid.

2.1. Standard Merging

Before calculating vector velocities from the available data set, a grid needs to be defined. Figure 1a represents the experimental data set: A radial velocity is measured in each elementary cell defined by a beam direction and a gate number. The dimension of a cell in the standard mode of operation is 45 km in range and variable in the transverse direction as a function of range.

2.1.1. The grid. The standard grid is defined by the intersection of radar beams from two radars, as shown in Figure 1b. The common area of two beams defines a "diamond." The radial velocities falling into this diamond are averaged for each radar, and the mean velocity vector is computed from these two averaged radial velocities. Each radar being scanned in 16 different directions, a two-dimensional map contains 256 potential velocity vectors. The spatial resolution depends on the azimuthal separation between beams. As the azimuthal width of a cell increases linearly with distance from the radar, the spatial resolution of this grid is not constant and varies from about 60 km at 1000 km to about 150 km at 2500 km.

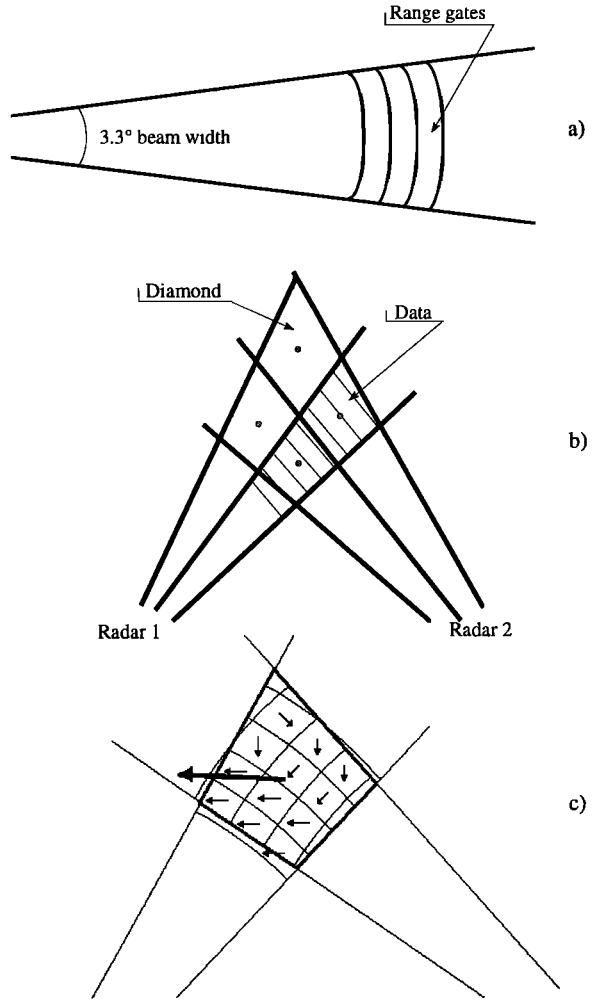


Figure 1. Schematic view of (a) the experimental data set with several gates in one radar beam, (b) the standard merging grid, and (c) the high-resolution grid.

The main advantage of this grid is that the resolution takes into account the increase of the azimuthal beam width with range. Therefore all velocity vectors are mutually independent. One radial velocity measurement is used in only one diamond.

2.1.2. Velocity vector computation. The first step in combining radial velocities to derive two-dimensional vectors is to associate a diamond to each radial velocity measurement.

SuperDARN radars are taking advantage of HF wave refraction in the ionosphere in order to achieve perpendicularity between the wave vector and the Earth's magnetic field lines in the auroral zone and polar cap. Without knowledge of the electron density profile, radar echoes cannot be exactly localized. The simplest approximation is straight-line propagation to an assumed altitude. This technique has been checked by *Villain et al.* [1984] and later by *Baker et al.* [1986]. Both groups of authors have estimated the localization error, for an assumed altitude of 300 km, based on comparison with ray tracing in realistic ionospheric models. In each case the error was estimated to be smaller than 30-40 km, i.e., smaller or of the order of a standard range gate. This result has been confirmed on a statistical basis by *André et al.* [1997].

In the standard merging algorithm [*Cerisier and Senior*, 1994], an assumption for the propagation is used, based on the *Breit and Tuve* [1926] theorem. This theorem states that the time delay along the real curved path in the ionosphere is equal to the delay to a virtual altitude, situated vertically above the real height, and along a straight line in free space. This theorem is subject to the condition that both rays have the same elevation angle at the radar site. Unfortunately, in the general case the elevation angle is not known, and a virtual altitude has to be assumed. In addition, the real altitude is never known and also has to be assumed. The standard default values are 400 and 325 km for the virtual and real heights, respectively.

From the time delay between transmission and reception of the radar pulse, the backscatter area is then localized, and a diamond number is assigned to individual data points. Radial velocities from each radar measured in range gates belonging to the same diamond are then averaged. From the averaged velocities measured by each radar, the resultant velocity for that diamond is calculated and is assigned to the "center" of the diamond, i.e., the point at which the centerlines of the two intersecting beams meet.

Whatever the hypothesis used to localize the scattering point, the expected error is much lower than the mean spatial resolution of the grid. Through the averaging process, the localization error on the radial velocity is smoothed and does not affect significantly the determination of velocity vectors. This means that the standard grid is rather insensitive to localization errors.

In order to compute the velocity vector, one needs to know the magnetic field vector and the wave vector inside the diamond. The magnetic field is given by the International Geomagnetic Reference Field (IGRF) 95 magnetic field model. The velocity vector is defined by the set of equations (1) where $\vec{b}$ is the unit vector along the magnetic field, $\vec{k_i}$ are the unit wave vectors transmitted from the radars 1 and 2, and V_i are the measured Doppler velocities.

$$\begin{aligned} \vec{k_1} \cdot \vec{V} &= V_1 \\ \vec{k_2} \cdot \vec{V} &= V_2 \\ \vec{b} \cdot \vec{V} &= 0 \end{aligned} \tag{1}$$

These equations define the two components of the velocity vector perpendicular to the magnetic field.

2.2. The High-Resolution Grid

We have defined a high-resolution grid using the intersection of measurement cells, as shown in Figure 1c. This figure shows the intersection of two different beams, defining one standard diamond. Inside this diamond are shown several measurement cells as they are defined by the range gates. This configuration, i.e., 3x4 radar gates in a diamond, is typical of diamonds situated far from the radar, at a distance of the order of 2500 km. Figure 1c clearly shows the increase in resolution to be expected from the use of the high-resolution grid, but it also illustrates one of its limitations. As discussed previously, the localization error can be of the order of the size of a grid cell, and therefore it becomes necessary to study this error in more detail.

In the high-resolution grid, the dimension of the cells is constant whatever the distance to the radars. The evaluation of the velocity vector in the cells situated at the same distance from a given radar is based on a single radial velocity measurement from that radar. Therefore the vectors are interdependent. This appears very clearly in Figure 1c. This interdependency increases with the distance to the radars. This problem can be partly overcome by the use of a high-resolution spectral analysis which is able to extract several velocities from a single autocorrelation function (ACF). Following *Barthes et al.* [1998], the multiple signal classification (MUSIC) method has been selected.

2.3. Localization Error

In order to estimate the error of localization, we follow the method used by *André et al.* [1997]. In that paper, the authors have used a ray-tracing program [*Jones and Stephenson*, 1975; *André et al.*, 1994] to localize radar backscatter in a statistical sense. Using a series of representative ionospheric density profiles, the authors have estimated the localization error introduced by the hypothesis considered by *Villain et al.* [1984] and by *Baker et al.* [1986]. Their results are in agreement with these previous studies.

Here we perform the same analysis in order to evaluate the error introduced by the hypothesis used in the standard merging method, i.e., a straight-line propagation to a virtual altitude of 400 km followed by a projection to the real altitude of 325 km. One thus estimates the field line on which backscatter occurs. The group path required to probe the same magnetic field line is determined by ray tracing. Then the error is defined as the difference between these two values of the group path (the group path associated with the propagation hypothesis is substracted from the one associated with the simulation). This error is computed for several frequencies and for 10 different ionospheric models, representative of the various electron density profiles characteristic of the high-latitude ionosphere. These simulations suppose a direct propagation path in the magnetic meridian and with a backscatter originating from the F region [*André et al.*, 1997].

Figure 2a shows the error calculated along the propagation path and averaged over the radar frequencies (11, 12, and 14 MHz) and over the 10 ionospheric density models. The error bars give the variance of those mean values, and the dashed lines show the maximum and minimum values obtained throughout all the ray-tracing computations. This figure shows that the localization error is approximatively constant along the propagation path and that its mean value is of the order of 55 km, with a variance of about 10 km. Figure 2b shows that this error can be minimized by changing the virtual altitude to 200 km and the real altitude to 175 km. In this case, the maximum localization error is 20 km. As mentioned previously, these estimations do not take into account either strong electron density perturbation resulting from precipitations or the 1.5-hop propagation mode which is sometimes observed in the radar data. Therefore, in the general case, we can at large ranges consider that lowering the virtual height from 400 to 200 km reduces the localization error to the order of magnitude of the spatial resolution in the radial direction.

However, in contrast to the insensivity of the standard merging grid to error, this localization error is critical in the case of the high-resolution grid, whatever the choice (within reasonable limits) of the virtual and real heights. In order to consider all possible localization errors, several configurations should be computed by shifting the data. The maximum shift amplitude considered here is of the order of the localization error found, i.e., one radial gate (45 km). In order to reduce the computation time, we make the hypothesis that the shift needed is the same over the whole radar field of view, as observed in Figure 2. In conclusion, possible localization errors are taken into account by computing three different maps corresponding to three different shifts (+1, 0, -1 gate) applied to all radial velocities.

2.4. High-Resolution Spectral Analysis

We have shown that the high-resolution grid implies that the same radial velocity measured by the radar in one range gate is used to compute several velocity vectors. Therefore the resulting vectors are not totally independent. In order to reduce this artificial smoothing, one has to increase the number of radial velocities deduced from the radar data.

From the SuperDARN multipulse transmission scheme, the real-time data processing computes 17 points of the complex autocorrelation function (ACF) of the backscattered signal. As described by *Villain et al.* [1987], the Doppler velocity is obtained from the fit of the ACF phase, and the spectral width is obtained from the fit of the ACF power. The fitted model assumes a spectrum resulting from only one velocity component corresponding to a linear variation of the ACF phase as a function of time. *Barthes et al.* [1998] have shown that this is not always the case and that the spectrum can include several components. *Schiffler et al.* [1997] have indeed related multicomponent spectra to small scale vortices (10 km) near the projection of the low-latitude boundary layer.

Multicomponent spectra can be used to reduce the interdependency of velocity vectors. However, the resolution of the Fourier transform is not sufficient, owing to the limited number of points in the ACF. On the contrary, high-resolution analysis can be achieved by the MUSIC method, which has

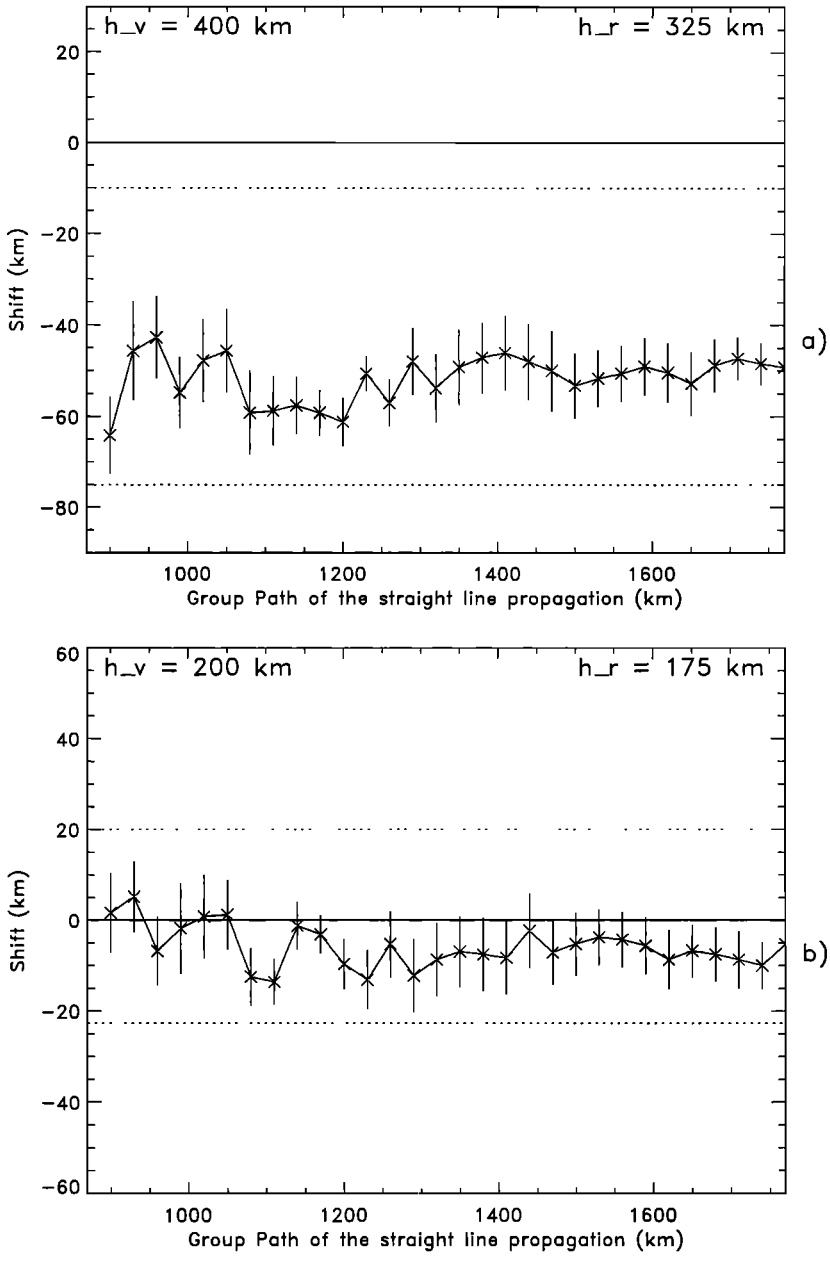


Figure 2. Localization error along the propagation path for a virtual altitude of (a) 400 km and (b) 200 km.

been successfully applied to SuperDARN by *Barthes et al.* [1998]. These authors have shown that the method is very sensitive to data quality, and severe criteria of applicability have been defined. Owing to these selection criteria, however, the number of multicomponent spectra is rather limited. For example, when applying this analysis to a convection reversal where multicomponent spectra are expected close to the velocity shear, a significant enhancement of the probability of observing such spectra is effectively obtained, but with a maximum probability of only 10%.

In order to reduce the dependency between velocity vectors the MUSIC algorithm is applied to extract the complete spectrum from each ACF. If a multicomponent spectrum is obtained in one radar cell, a velocity vector is computed for each component. Several vectors can therefore be obtained in one grid point.

2.5. Selection Hypothesis

The solutions proposed above to solve the questions raised by the implementation of the high-resolution grid lead to several possible velocity vectors at one grid point (one gate shift and multicomponent spectra). Consequently, a selection criterion has to be defined to choose among the several high-resolution maps obtained.

In the F region, the plasma moves in the $\vec{E} \times \vec{B}$ direction, where $\vec{E}$ is the convection electric field and $\vec{B}$ is the Earth's magnetic field. This two-dimentional motion has been shown to be divergence-free [e.g.,*Ruohoniemi et al.*, 1989]. This hypothesis is not scale dependent, and so is then true in the whole auroral oval as well as in one grid cell.

$$\sum_{i=1}^{N_{vectors}} \vec{\nabla} \cdot \vec{V_i} = \vec{\nabla} \cdot \vec{V_i} = 0 \qquad (2)$$

Taking into account this property, it is possible to select the configuration which minimizes the velocity divergence. Such a velocity divergence can come from experimental features (spatiotemporal integration in one radar gate, temporal variation of the convection between beams, errors in the velocity determination,etc.). In order to avoid large and opposite divergences (large and opposite experimental errors) we use the following selection criteria :

$$\sum_{i=1}^{N_{vectors}} |\vec{\nabla} \cdot \vec{V_i}| \text{ minimum} \qquad (3)$$

The first step is to compute a reference map with no multicomponent spectra and no shift due to localization errors. Then, for each global shift of the map (0, -1, +1 range gate), the velocity divergence is minimized by choosing between the various multicomponent spectra. Finally, we retain the map with minimum divergence. At this point, we obtain a high-resolution map of the ionospheric convection, which takes into account possible localization errors, reduces the interdependency between velocity vectors, and minimizes the magnitude of the velocity divergence.

2.6. Evaluation of the Method

Following the work of *Wei and Lee* [1990], *Thorolfsson* [1996] has modeled the ionospheric signature of a flux transfer event (FTE). This consists of a double convection vortex that travels at the same plasma velocity as in the central part of the vortex. Here we use this model to reproduce a known signature and test the ability of the high-resolution method to resolve small-scale structures. In the following, the vortex is traveling through the radar field of view at a fixed velocity of 1.5 km/s, typical of FTEs. By varying the size of this simulated double vortex, it will be possible to determine the limits of the high-resolution method and compare with the results given by the standard mapping method.

In order to simulate the MUSIC results, each radar range cell is subdivided into three parts, and the radial velocities corresponding to the model are computed for each subdivided cell. We assume that the central part of the elementary cell is the radial velocity deduced from the standard ACF analysis and that the two others are the new radial velocities found by the MUSIC method.

2.6.1. Scale length of 500 km. Figure 3a shows the instantaneous velocity field of a structure sitting in the middle of the radar field of view as projected on the high-resolution grid before velocity projection along the radar beams. The structure has a scale length of 500 km. The points represent the grid points, and the lines represents the velocity direction and amplitude. This map defines the reference map. Figure 3a shows the well-defined double vortex structure, with plasma velocities of 1.5 km/s in the center. Figure 3b shows the map deduced from the standard analysis and exhibits the same characteristics. Figure 3c presents the map obtained with the high-resolution method. The same structure is seen but with a much better definition than in Figure 3b. The slight differences between Figures 3a and 3c are due to the fact that the structure is traveling through the radar fields of view, while projections along the radar beams are made sequentially to mimic the real operation of the radars, which scan sequentially through all the beams. Therefore Figure 3c does not show the instantaneous signature of the FTE as in Figure 3a. From the similarities between Figure 3a and 3c, we can conclude that the high-resolution algorithm re-

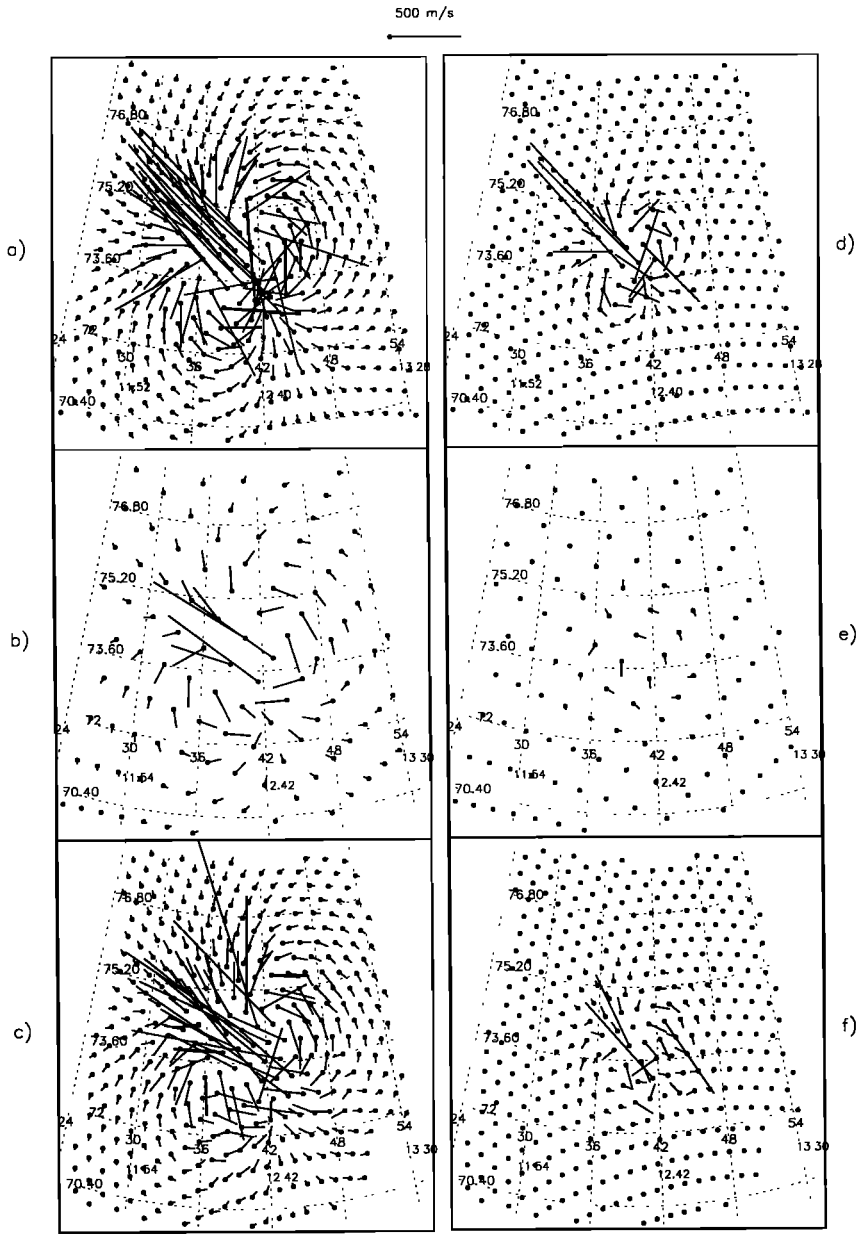


Figure 3. Simulation of a double vortex convection pattern. (a) Reference double vortex with a scale size of 500 km. (b) Simulated measurements processed with the standard merging algorithm. (c) Simulated measurements processed with the high-resolution algorithm. (d, e, f) Same as Figure 3a, 3b, and 3c, but for a scale size of 250 km.

produces correctly the ionospheric convection, with a better resolution than the standard one.

2.6.2. Scale length of 250 km. Figures 3d, 3e, and 3f present the results obtained when the size of the structure is reduced by a factor of 2, keeping the same central velocity. Again, the reference map (Figure 3d) defines the double vortex signature. Now one clearly observes that the resolution of the standard merging method is not sufficient to reproduce this structure. The velocities inside the structure

are not large enough, owing to averaging in the diamond center. Some of them are in a wrong direction, and the double vortex structure does not appear at all. The only conclusion which can be derived from this map is that a small undefined structure probably exists in the convection. On the contrary, the high-resolution map still exhibits the most important characteristics of the event. We observe the large velocities in the center of the structure, and the double vortex is well defined. Of course, this map is not as well defined as the reference one, but the imprecisions can again be attributed to the time averaging effect.

In summary, the high-resolution method can reasonably well identify structures with a typical scale size of 250 km and gives partial information when the scale is going toward the grid scale size. Therefore this high-resolution method is able to give more information than the standard one on structures which have a typical scale size between approximatively 500 and 200 km.

3. Small-Scale Structures in the Ionospheric Convection

In this section, the high-resolution algorithm is applied to SuperDARN data. Two typical examples are shown in which small-scale structures can be resolved, representing a convection reversal and a convection vortex, respectively.

3.1. Convection Reversal

In this example, we use data from the Saskatoon/Kapuskasing radar pair, measured in the dusk sector on March 7, 1995, between 0102 and 0105 UT. Figure 4 shows the convection maps obtained with the standard merging method (Figure 4a) and the high-resolution method (Figure 4b). These two maps show, in geomagnetic coordinates, a well-defined convection reversal, sketched by the superimposed bold arrow.

In Figure 4a the convection reversal is clearly evident, but the location of the velocity shear is not well defined. This reversal seems to be characterized by a very smooth velocity gradient, with a typical scale length of the order of 250 km. With the high-resolution method, the convection reversal exhibits much sharper characteristics. The velocity shear is very well localized, as shown by the dashed line. From this map, the gradient scale length, in the direction perpendicular to the shear, can be estimated to be about 90 km. One can note here that the smoothing effect of the averaging process used in the standard merging method is removed by the high-resolution algorithm.

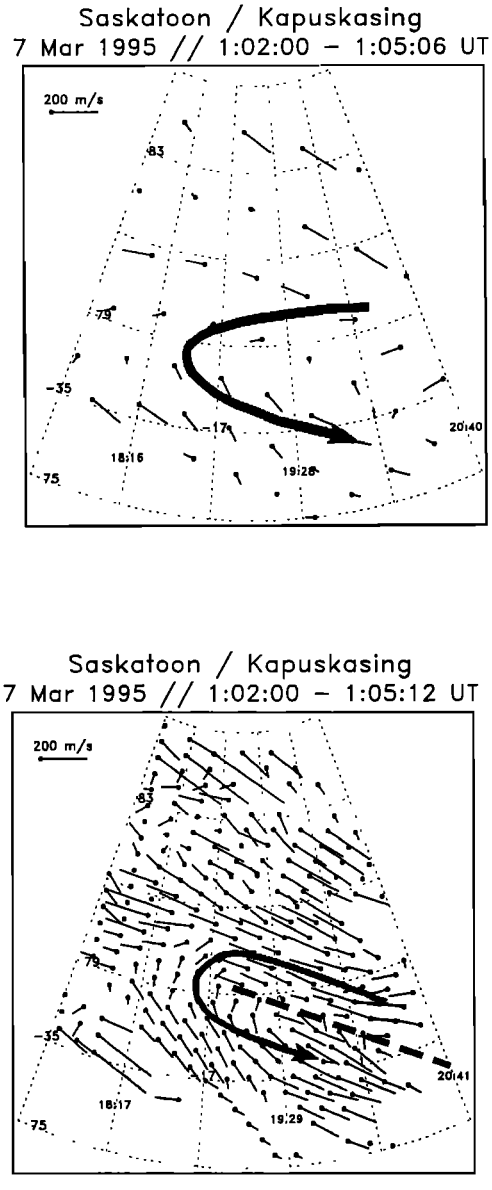


Figure 4. A convection reversal measured by the Saskatoon/Kapuskasing radar pair as reproduced by (a) the standard merging method and (b) the high-resolution merging method. The bold arrow sketches the observed convection pattern, and the dashed line indicates the location of velocity shear.

Figure 4b also illustrates the fact that all velocity vectors are not independent. Several vector groups are identical or close to identical. This is particularly evident at high latitudes (82°magnetic latitude (MLAT), between 1930 and 2030 magnetic local time (MLT)), where several vectors have the same direction and amplitude. In this region, the MUSIC method was not able to extract multicomponent spectra. This may be due to poor data quality, but it can also result from a homogeneous convection zone, without any velocity structure.

This example shows clearly the benefits and limitations of the method. It is able to define more precisely small-scale structures and sharp variations in the convection and to quantify the structure scale lengths. Nevertheless, it cannot solve totally the velocity vector dependence problem when regular flows are present.

3.2. Vortex in the Convection

The second example was obtained on March 8, 1995, between 0059 and 0102 UT, by the Saskatoon/Kapuskasing radar pair when a mesoscale vortex is observed in the 81°MLAT and 1930 MLT sector.

Figure 5a shows the structure mapped with the standard merging method. A vortex is observed to be embedded in an eddy flow. Despite the fact that this vortex is not perfectly defined, we can infer a typical scale length of the order of 200 km. Figure 5b shows the same vortex mapped by the high-resolution merging method. As in Figure 5b, the vortex is embedded in an eddy flow, but the localization of the vortex center at about 81°and 1930 MLT is more precise, and its typical scale size is inferred to be of the order of 100 km. Around this structure, in the upper part of the field of view, the plasma motion is well defined and shows a large convection reversal.

Again, the high-resolution method gives a more detailed description of the convection pattern. The typical scale size is evaluated with greater confidence, and the field-aligned currents associated with this vortex may be estimated more precisely with the method developed by *Sofko et al.* [1995].

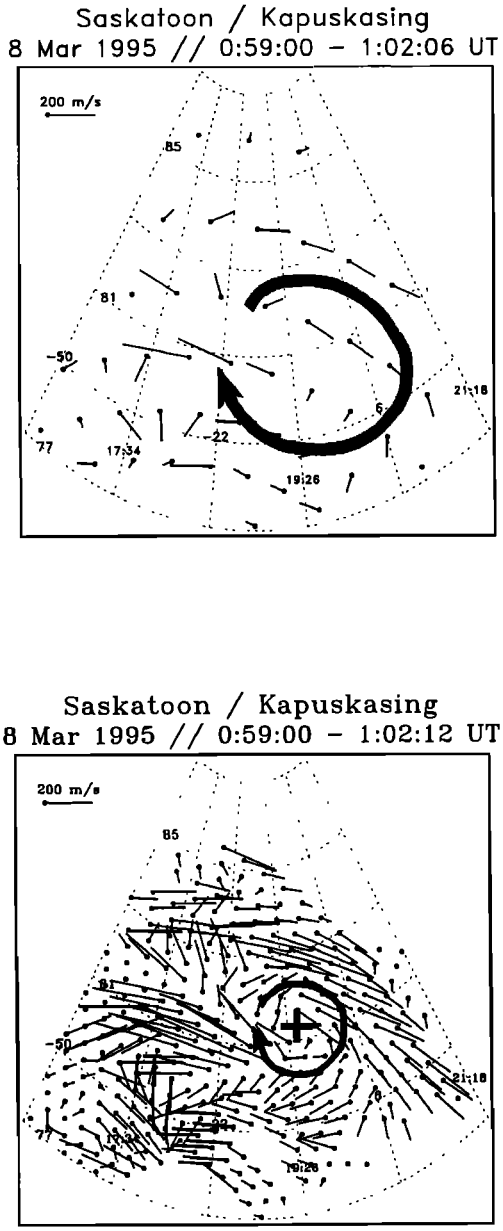


Figure 5. A vortex measured by the Saskatoon/Kapuskasing radar pair as reproduced by (a) the standard merging method and (b) the high-resolution merging method. The bold arrow sketches the observed convection pattern, and the cross shows the center of the vortex.

4. Discussion

The merging method developed in this paper is based on several hypotheses, which are now discussed. First of all, the high-resolution spectral analysis is made with the MUSIC method. Because of its great selectivity, this method does not provide a large number of multipeaked spectra. Typically,

the probability of obtaining a double-peaked spectrum is at most 10% [*Barthes et al.*, 1998], a figure which is considerably smaller than the 100% probability used in the simulation. These figures lead us to expect to reduce the mean divergence by a factor much smaller than 45%, as obtained in the simulated map. A consequence of this limited number of multipeaked spectra is also the dependence of neighboring velocity vectors, which share a common radial velocity component. In the future, we may hope to reduce the dependence of the vectors by measuring more accurately the autocorrelation function or by using a more efficient spectral analysis method.

Possible localization errors are taken into account by computing three different maps, corresponding to three different shifts applied to all radial velocities and over the whole radar field of view. Because the estimated localization error is based on a statistical study, we have supposed that the average ionospheric density profile is the same for each radar beam, i.e., is independent of the azimuth. This strong hypothesis is not generally true, and we can easily suppose that a meridional beam will not experience the same ionospheric density profile as a zonal one. The ionospheric models used in this simulation are supposed to be representative of both dayside and nightside conditions [*André et al.*, 1997]. We can consider that this variability is a good estimate of the azimuthal variability of the ionospheric density profile. Then, the fluctuation of the localization error with respect to the ionospheric model can give an estimate of its variation with the azimuth. This error is quantified by the error bars in the Figures 2a and 2b and is of the order of 10 km, less than one range gate. Then, in a first approximation, the application of the same shift over the whole radar field of view is acceptable. Of course, a more rigorous treatment should consider different shifts for different beams.

The computation of a velocity map leads to the selection of several new radial velocities taken from the multipeaked spectra and of one range offset which corresponds to the localization adjustment. The influence of the number of new velocities determined by MUSIC on the determination of the offset can be questionned. Using the particular case simulated above, the selected offset has been modified when the proportion of multipeaked spectra did represent at least 50% of the radar data. Thus the offset determination could depend on the expected proportion of multipeaked spectra on a real convection map. In most of the observed cases, this proportion never reached more than 10% [*Barthes et al.*, 1998]. Thus one can expect that this value always remains below 50%, and one concludes that the presence of multipeaked spectra should not influence the determination of the range offset.

At last, we have supposed that all the velocities measured in one range cell represent the convection velocity. This hypothesis can be wrong if the velocity field is made of small-scale structures superposed on a larger-scale convection, as hypothesized by *Schiffler et al.* [1997] with a specific model of vortices. The problem can be serious if, in addition, the scattering cross section is larger in the small-scale structures than in the large-scale convection. If the measured radial velocity components are all polluted by the small-scale structure, it is clear that the resulting velocity map will no longer represent the large-scale convection, but that it will include a degree of spatial aliasing. However, we may also expect an increase in the divergence in that case. On the contrary, if at least one of the measured velocity represents the convection, we may expect that it will lead to a smaller divergence.

5. Conclusions

We have presented a method which optimizes the spatial resolution of the velocity maps deduced from SuperDARN data and extracts more information on small-scale structures ($L \approx 200$ km) present in the ionospheric convection. We first have defined the high-resolution grid on which the velocity vectors are computed and have pointed out the difficulties inherent in this grid. An estimate of the localization error has been given and has been shown to be of the order of the radial resolution of the SuperDARN radars (one grid step). The elementary cells and the grid used imply a velocity vector dependence that we have reduced by using the MUSIC high-resolution spectral analysis. In order to give reliable results, the method is very selective, and, as a result, all vectors are not totally independent. The solutions found imply a selection between several maps with the help of a physical criterion. The selected map minimizes the sum of the divergence magnitudes. With simulated SuperDARN data, we have illustrated the limitations of the method. We conclude that this method gives more information than the standard one for structures with a typical scale size between 250 and 500

km. Finally, we have illustrated the method with experimental SuperDARN data, showing a convection reversal and a vortex. In both cases, the method extracts more detailed information on small-scale size features.

In conclusion, when applied to SuperDARN radar data, the high-resolution merging algorithm gives access to small-scale structures in the ionospheric convection. This can be very useful for a better understanding of perturbations such as the ionospheric signature of flux transfer events, traveling convection vortices, or the highly structured convection which prevails during northward interplanetary magnetic field time periods.

Acknowledgments. The Kapuskasing HF radar is funded by NASA under grant NAG5-1099. The Saskatoon HF radar is funded by an NSERC Canada Collaborative Special Project grant.

References

André, R., J.-P. Villain, and F. Germain, Ray-tracing program, *Tech. Rep. LPCE/NTS/022.A*, 42 pp., Lab. Phys. Chim. Environ., Cent. Nat. de la Rech. Sci., Orléans, France, 1994.

André, R., C. Hanuise, J.-P. Villain, and J.-C. Cerisier, HF radars: Multifrequency study of refraction effects and localization of scattering, *Radio Sci., 32*, 153-168, 1997.

Baker, K.B., R.A. Greenwald, A.D.M. Walker, P.F. Bythrow, L.J. Zanetti, T.A. Potemra, D.A. Hardy, F.J. Rich, and C.L. Rino, A case study of plasma processes in the dayside cleft, *J. Geophys. Res., 91*, 3130-3144, 1986.

Barthes, L., R. André, J.-C. Cerisier, and J.-P. Villain, Separation of multiple echoes using a high-resolution spectral analysis for SuperDARN HF radars, *Radio Sci., 33*,1005-1017,1998.

Breit, G., and M.A. Tuve, A test of the existence of the conducting layer, *Phys. Res., 28*, 554, 1926.

Bristow, W.A., et al., Observations of convection vortices in the afternoon sector using the SuperDARN HF radars, *J. Geophys. Res., 100*, 19,743-19,756, 1995.

Cerisier, J.-C. and C. Senior, *Merge: A Fortran Program*, 40 pp., Cent. d'Etude des Environ. Terr. et Planét., Cent. Nat. de la Rech. Sci., St-Maur, France, 1994.

Greenwald, R.A., et al., DARN/SuperDARN: A global view of the dynamics of the high-latitude convection, *Space Sci. Rev.,71*, 761, 1995a.

Greenwald, R.A., W.A. Bristow, G.J. Sofko, C. Senior, J.-C. Cerisier, and A. Szabo, Super Dual Auroral Radar Network radar imaging of the dayside high-latitude convection under northward interplanetary magnetic field: Toward resolving the distorted two-cell versus multicell controversy, *J. Geophys. Res., 100*, 19,661-19,674, 1995b.

Greenwald, R.A., J.M. Ruohoniemi, W.A. Bristow, G.J. Sofko, J.-P. Villain, A. Huuskonen, S. Kokubun, and L.A. Frank, Mesoscale dayside convection vortices and their relation to substorm phase, *J. Geophys. Res., 101*, 21,697-21,713, 1996.

Jones, R.M., and J.J. Stephenson, A versatile three dimensional ray tracing program for radio waves in the ionosphere, *Tech. Rep. OT 75-76*, 185 pp., Off. of Telecommun., U.S. Dep. of Commer., Boulder, Colo., 1975.

Lewis, R.V., M.P. Freeman, A.S. Rodger, G.D. Reeves, and D.K. Milling, The electric field response to the growth phase and expansion phase onset of a small isolated substorm, *Ann. Geophys., 15*, 289-299, 1997.

Rodger, A.S., and M. Pinnock, The ionospheric response to flux transfert events: The first few minutes, *Ann. Geophys., 15*, 685-691, 1997.

Ruohoniemi, J.M., R.A. Greenwald, K.B. Baker, J.P. Villain, C. Hanuise, and J. Kelly, Mapping high-latitude plasma convection with coherent HF radars, *J. Geophys. Res., 94*, 13,463-13,477, 1989.

Schiffler, A., G. Sofko, P.T. Newell, and R.A. Greenwald, Mapping the outer LLBL with SuperDARN double-peaked spectra, *Geophys. Res. Lett., 24*, 3149-3152, 1997.

Sofko, G.J., R. Greenwald, and W. Bristow, Direct determination of large-scale magnetospheric field-aligned currents with SuperDARN, *Geophys. Res. Lett., 22*, 2041-2044, 1995.

Thorolfsson, A., it Transfert de flux magnétique intermittents entre le vent solaire et la magnétosphère : Théorie et modélisation des signatures, 54 pp., Cent. d'Etude des Environ. Terr. et Planét., Cent. Nat. de la Rech. Sci., St-Maur, France, 1996.

Villain, J.-P., R.A. Greenwald, and J.F. Vickrey, HF ray tracing at high latitudes using measured meridional electron density distributions, *Radio Sci., 19*, 359-374, 1984.

Villain, J.-P., R.A. Greenwald, K.B. Baker, and J.M.

Ruohoniemi, HF radar observations of *E* region plasma irregularities produced by oblique electron streaming, *J. Geophys. Res., 92*, 12,327-12,342, 1987.

Wei, C.Q., and L.C. Lee, Ground magnetic signatures of moving elongated plasma clouds, *J. Geophys. Res., 95*, 2405-2418, 1990.

Yeoman, T.K., and H. Luhr, CUTLASS/IMAGE observations of high-latitude convection features during substorms, *Ann. Geophys., 15*, 692-702, 1997.

R. André and J. P. Villain, Laboratoire de Physique et Chimie de l'Environnement, CNRS, 3A Avenue de la Recherche Scientifique, 45071 Orléans cedex 2, France.

L. Barthes, J. C. Cerisier, C. Senior, and A. Thorolfsson, Centre d'Etude des Environnements Terrestres et Planétaires, CNRS, 4 Avenue de Neptune, 94107 Saint-Maur-des-Fossés Cedex, France.

C. Hanuise, Laboratoire de Sondage Electromagnétique de l'Environnement Terrestre, CNRS, Université de Toulon, BP 132, 83957 La Garde, France

(Received August 4, 1998; revised January 25, 1999; accepted April 7, 1999.)